Mechanism of the *Clostridium thermoaceticum* Pyruvate:Ferredoxin Oxidoreductase: Evidence for the Common Catalytic Intermediacy of the Hydroxyethylthiamine Pyropyrosphate Radical†

Saurabh Menon and Stephen W. Ragsdale*

Department of Biochemistry, Beadle Center, University of Nebraska, Lincoln, Nebraska 68588-0664

Received February 21, 1997; Revised Manuscript Received May 5, 1997⊗

ABSTRACT: The cofactor content and mechanism of pyruvate:ferredoxin oxidoreductase (PFOR) are controversial. By using rapid freeze−quench EPR and stopped-flow spectroscopy, the elementary steps that constitute the first half-reaction of the *Clostridium thermoaceticum* PFOR mechanism were elucidated. A hydroxyethyl−TPP (HE−TPP) radical was identified and characterized as a transient intermediate, and for the first time, the kinetic competence of this substrate-derived radical was demonstrated. When the *C. thermoaceticum* PFOR was reacted with pyruvate and CoA, it had a lifetime of only ∼100 ms. The results described here suggest that this radical intermediate is often not detected in studies of α-ketoacid oxidoreductases because it rapidly decays. It is postulated here that the HE−TPP radical is an intermediate in the mechanism of all PFORs irrespective of the number of 4Fe-4S clusters and will be detected in all PFORs when rapid mixing methods are used. The *C. thermoaceticum* PFOR was shown to contain two 4Fe-4S clusters, as concluded earlier [Wahl, R. C., & Orme-Johnson, W. H. (1987) *J. Biol. Chem. 262*, 10489−10496]. The first reductive half-reaction was shown to involve the following steps: (i) reaction with pyruvate with PFOR to form the hydroxyethylidene−TPP intermediate; (ii) one-electron transfer to reduce one of the two Fe_4S_4 clusters and yield the HE−TPP radical; and, (iii) reaction with CoA resulting in formation of acetyl-CoA, rapid decay of the HE−TPP radical intermediate, and reduction of the second Fe_4S_4 cluster. Thus, at the end of the first half-reaction, the two Fe_4S_4 clusters are fully reduced. The rate of the third step was found to depend on the CoA concentration (k = 35 per s at saturating concentrations of CoA); however, in its absence, this step was slower by ∼4400-fold.

Pyruvate:ferredoxin oxidoreductase (PFOR)[1] is one of several enzymes, including pyruvate dehydrogenase (PDH), pyruvate decarboxylase (PDC), pyruvate oxidase, and pyruvate:formate lyase, that can initiate pyruvate catabolism. PDH links glycolysis to the tricarboxylic acid cycle; whereas, PDC plays a key role in ethanol fermentation by converting pyruvate to acetaldehyde. PDH and PFOR catalyze the oxidative decarboxylation of pyruvate to acetyl-CoA and CO_2. PDH contains lipoamide and specifically reduces NAD^+; whereas, PFOR lacks lipoamide and reduces a number of electron carriers, including ferredoxin (Fd), flavodoxin, and viologen mediators, but not pyridine nucleotides. Present in all three kingdoms (*Archaea*, Bacteria, and Eukaryotes), PFOR apparently was designed for anaerobic fermentative metabolism since, so far, it has never found in an organism containing mitochondria (Hrdy' & Müller, 1995).

The oxidative decarboxylation of pyruvate by PFOR occurs according to the following half-reaction (eq 1):

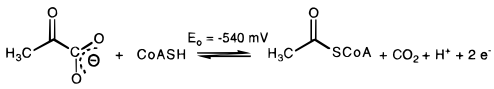

(1)

In anaerobic acetogenic bacteria like *Clostridium thermoaceticum*, PFOR links glycolysis to the Wood/Ljungdahl pathway. In this pathway, PFOR interacts with the bifunctional enzyme, CO dehydrogenase/acetyl-CoA synthase (CODH/ACS), to convert the carboxyl group of pyruvate to the carbonyl group of acetyl-CoA (Drake *et al.*, 1981; Menon & Ragsdale, 1996a). This is a multistep reaction sequence in which, first, PFOR catalyzes the decarboxylation of pyruvate to form acetyl-CoA and CO_2. Then, CO_2 is reduced to CO by CODH/ACS; subsequently, CO generated *in situ* combines with the ACS active site to form a paramagnetic adduct that has been called the NiFeC species, and the bound carbonyl group combines with a bound methyl group and CoA to generate acetyl-CoA (Menon & Ragsdale, 1996a). Presumably, a similar mechanism allows certain methanogens to grow on pyruvate as a carbon source (Bock *et al.*, 1994; Rajagopal & LeGall, 1994; Bock & Schönheit, 1995).

PFOR is a member of the α-ketoacid oxidoreductase family. Three types of α-ketoacid oxidoreductases, differing in subunit composition, have been described and were proposed to form a functionally and structurally related superfamily (Adams & Kletzin, 1996). The reaction mech-

† This work was supported by NIH Grant GM39451 (S.W.R.).

* Address correspondence to Department of Biochemistry, Beadle Center, University of Nebraska, Lincoln, Nebraska 68588-0664. Phone: 402-472-2943. Fax: 402-472-7842. Email: sragsdal@unlinfo.unl.edu.

⊗ Abstract published in *Advance ACS Abstracts*, July 1, 1997.

[1] Abbreviations: SDS−PAGE, sodium dodecyl sulfate-polyacrylamide gel electrophoresis; CODH/ACS, CO dehydrogenase/acetyl-CoA synthase; PFOR, pyruvate:ferredoxin oxidoreductase; PDH, pyruvate dehydrogenase; PDC, pyruvate decarboxylase; TPP, thiamin pyrophosphate; HE−TPP, hydroxyethyl−TPP; MES, 2-(*N*-morpholino)ethanesulfonic acid; FQ-EPR, rapid freeze−quench EPR.

S0006-2960(97)00403-0 CCC: $14.00 © 1997 American Chemical Society

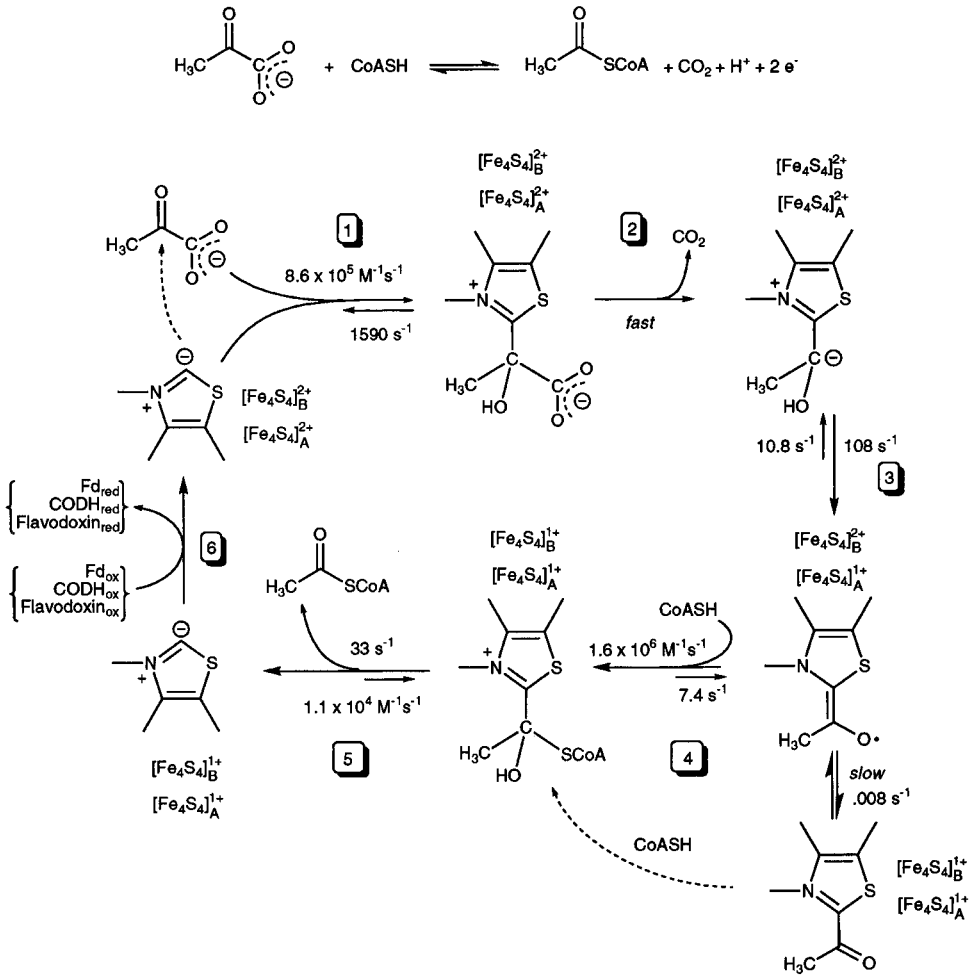

FIGURE 1: Proposed reaction mechanism for the oxidation of pyruvate by PFOR illustrating (1) pyruvate binding, (2) formation of hydroxyethylidene−TPP intermediate, (3) formation of the HE−TPP radical and reduction of cluster A, (4) CoA binding and reduction of cluster B, (5) formation of acetyl-CoA and regeneration of the TPP anion, and (6) reduction of external electron acceptors. The predominant Fd in *C. thermoaceticum* is an eight Fe-Fd that can accept two electrons (Elliott & Ljungdahl, 1982).

anism of this class of enzymes has been controversial. The results described here are consistent with the mechanism described in Figure 1 for the PFORs. The first two steps in the reaction mechanism are common for PFOR, PDH, PDC, and thiamine pyrophosphate (TPP) in solution. These enzymes react with pyruvate to form a pyruvoyl−TPP adduct (step 1) which decarboxylates to generate the hydroxyethylidene−TPP intermediate (step 2).

At step 3, the PDH, PDC, and PFOR mechanisms diverge. Our results indicate that, for the *C. thermoaceticum* PFOR, one electron is transferred from hydroxyethylidene−TPP to one of the two FeS clusters, which yields a pyruvate-derived radical. Detection of this radical when the *Halobacterium salinarium* (formerly *halobium*) PFOR was reacted with pyruvate led to a proposed mechanism that included a hydroxyethyl−TPP (HE−TPP) radical intermediate (Cammack *et al.*, 1980; Kerscher & Oesterhelt, 1981). The radical was assigned as a HE−TPP radical because it arises after the TPP-dependent decarboxylation of pyruvate, but before CoA reacts, and because EPR spectroscopic studies clearly showed that the protons from C-3 of pyruvate are part of the spin $S = 1/2$ spin system. Although direct spectroscopic evidence for the presence of the TPP moiety in the spin system is not available, we feel that sufficient evidence supports this assignment and will follow convention in referring to the substrate-derived radical as the HE−TPP radical throughout this paper. A hydroxyalkyl−TPP radical also has been detected with other PFORs (Smith *et al.*, 1994; Pieulle *et al.*, 1995) and α-ketoacid oxidoreductases (Mai & Adams, 1994; Heider *et al.*, 1996). The significance of this radical could be questioned since the kinetic competence of the hydroxyalkyl−TPP radical has not been previously demonstrated with any of the α-ketoacid oxidoreductases. Furthermore, this radical was not observed in studies of several other PFORs, including the one from *C. thermoaceticum* (Wahl & Orme-Johnson, 1987; Smith *et al.*, 1994; Moulis *et al.*, 1996). Two proposals to rationalize the apparent differences have been described. One is that the PFORs from members of the *Archaea* kingdom use a radical-based mechanism, but those from *Bacteria* follow a nonradical pathway (Blamey & Adams, 1993; Smith *et al.*, 1994). Another postulate is that PFORs containing an odd number of Fe_4S_4 clusters use a radical pathway, whereas, those having an even number use a mechanism lacking a radical intermediate (Pieulle *et al.*, 1995). The results described here provide a simple explanation for why this radical was not observed in some studies and lead us to suggest that this radical may be an intermediate in the mechanism of all PFORs.

Steps 4 and 5 involve transfer of one electron from the HE−TPP radical to another FeS cluster leaving an acetyl−TPP intermediate that undergoes cleavage by CoA to form acetyl-CoA. These steps leave the enzyme in the two-electron reduced state, with both FeS clusters reduced. Step 6 completes the catalytic cycle by oxidizing the enzyme. Fd

and flavodoxin are well-known electron acceptors for PFOR. PFOR was recently shown to be both an electron and CO_2 donor to CODH/ACS (Menon & Ragsdale, 1996a). CODH/ACS then converts CO_2 to CO, which is condensed with a bound methyl group and CoA to yield acetyl-CoA via the Wood/Ljungdahl pathway (Menon & Ragsdale, 1996a). The acetyl-CoA is used as a source of ATP through the actions of phosphotransacetylase and acetate kinase or as a source of cell carbon allowing these bacteria to grow autotrophically.

We used a combination of rapid kinetic and spectroscopic methods to elucidate the reaction mechanism of the *C. thermoaceticum* PFOR. Several elementary steps shown in Figure 1 were identified and quantified. We present strong evidence supporting the intermediacy of the HE−TPP radical intermediate. We suggest that this radical will be detected in all PFORs when rapid mixing methods are used and that all PFORs will be found to use a similar radical-based mechanism.

METHODS

Materials. N_2 (99.8%, from Linweld) was deoxygenated by passage through a heated column containing a BASF catalyst. Reagents were of the highest purity available. CD_3-pyruvate was synthesized as described (Seravalli, 1994), and the purity was confirmed by mass spectrometry.

Organism and Enzyme Purification. C. thermoaceticum strain ATCC 39073 was grown on glucose at 55 °C (Andreesen *et al.*, 1973). PFOR was purified as described (Wahl & Orme-Johnson, 1987) except that ion exchange chromatography was performed on a DEAE-Sephacel column and the enzyme was eluted with a 2 L linear gradient from 0 to 0.4 M NaCl in 1 mM TPP and 50 mM 3-(*N*-morpholino)propanesulfonic acid (MOPS) buffer (pH 7.5), hereafter called buffer A. Protein concentrations were routinely determined by the Rose Bengal method (Elliott & Brewer, 1978) using bovine serum albumin as a standard. The standard assay for PFOR activity that was used during enzyme purification contained 50 mM Tris-HCl (pH 7.5), 1 mM TPP, 10 mM sodium pyruvate, 1 mM CoA, and 10 mM methyl viologen in a final volume of 1 mL. PFOR concentrations are presented based on the protein being a dimer, which is its native quaternary structure (Drake *et al.*, 1981).

Metal, Sulfide, and Protein Measurements. We calibrated the Rose Bengal Assay by determining the total amino acid content of PFOR. The enzymatic activities, the protein contents (by the Rose Bengal assay), and the UV−visible spectra of two samples that differed by 4-fold in protein content were measured. These samples were then subjected to HCl vapor phase hydrolysis and total amino acid analysis on a Beckman 6300 analyzer.

Iron content was determined by plasma emission spectroscopy (Jones, 1977) and by nonheme iron analysis (Fish, 1988). Acid labile sulfur was determined as methylene blue (Cline, 1969). Iron and sulfide were determined independently in two separate preparations of enzyme.

EPR Spectroscopy. EPR spectra were recorded on a Bruker ESP 300E spectrometer equipped with an Oxford ITC4 temperature controller, a model 5340 automatic frequency counter (Hewlett Packard), and a Bruker Gaussmeter. Spin concentrations were measured by comparing the double integrals of the spectra with those of a 1 mM copper perchlorate standard. The spin intensities were independently measured for enzyme obtained from four separate protein preparations. The spectroscopic parameters are given in the figure legends.

The value of the power for half saturation of the EPR signal ($P_{1/2}$) was determined by measuring the signal intensity at different microwave powers and fitting the data to eq 2, where S and P refer to the signal amplitude and microwave power, respectively; A is a scaling factor; and b is defined as the inhomogeneity parameter (Rupp *et al.*, 1978).

$$\log S/(\mathrm{P})^{0.5} = \log A/(1 + P/P_{1/2})^{0.5b} \qquad (2)$$

Steady-State and Pre-Steady-State Kinetics Experiments. To determine the value of k_{cat}/K_m for viologen under steady-state conditions, the standard assay (above) was employed except that the viologen concentration was 50 μM and the pyruvate concentration was varied from 1 to 12.5 mM. The assays were performed at 25 °C and initiated by adding PFOR. The kinetic parameter k_{cat}/K_m was obtained by following the reaction to completion and fitting the data as increasing absorbance of reduced dye versus time to eq 3, which is the exponential form of the Michaelis−Menten equation for a first-order or pseudo-first-order reaction (Segel, 1975). In all of our experiments, methyl viologen was completely reduced, demonstrating the irreversibility of the reaction and indicating that the PFOR reaction satisfies the conditions for treating the data by eq 3. Furthermore, the values of k_{cat} and the K_m for methyl viologen were independently measured by initial velocity kinetics.

$$A = (A_i - A_0)\exp[-k_{cat}(t/K_m)] + A_i \qquad (3)$$

Rapid freeze−quench EPR (FQ-EPR) was performed essentially as described (Ballou, 1978) using an Update Instruments chemical/freeze−quench instrument with a computer-operated Model 745 controller. The temperature of the isopentane bath was maintained at −140 °C. The conditions used for performing EPR spectroscopy are described in the figure legends. Stopped-flow studies were performed on a DX.17MV Sequential Stopped-flow ASVD Spectrofluorimeter from Applied Photophysics (England) under anaerobic conditions as described earlier (Zhao *et al.*, 1995). The temperature of the mixing system was maintained at 25 °C by a water bath equipped with a circulating pump and continually bubbled with nitrogen. Data were fit to a single- or double-exponential equation using the software supplied by Applied Photophysics. The spectroscopic parameters are described in the figure legends. Stopped-flow and FQ-EPR data were analyzed using the software programs KINSIM and FITSIM (Barshop *et al.*, 1983; Zimmerie & Frieden, 1989). To simulate the stopped flow data, two phases with equal amplitude and an extinction coefficient of 7.4×10^3 M^{-1} cm^{-1}/cluster/phase was used ($\Delta\epsilon$).

RESULTS

Metal Content and Spectroscopic Properties. The *C. thermoaceticum* PFOR was found to contain 16 ± 1 g atm iron and 16 g atm of acid-labile sulfide/mol of dimeric protein. The stoichiometries of metals and sulfide were based on protein concentrations that were analyzed by a colorimetric method and by amino acid analysis. No other metals were detected in amounts greater than 0.2 g atm/mol

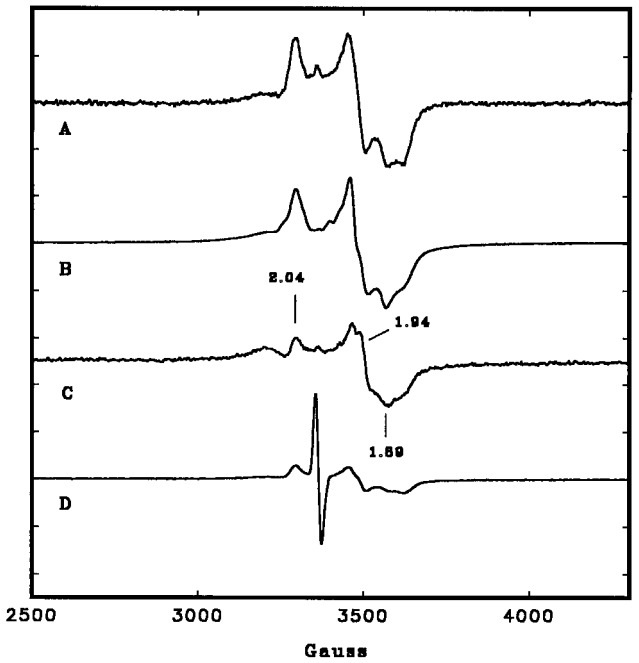

FIGURE 2: EPR spectra of PFOR. A solution containing 50 μM PFOR and 1 mM TPP in a final volume of 200 μL was incubated for 5 min with **(A)** 5 mM sodium dithionite, **(B)** 10 mM pyruvate and 1 mM CoA, **(C)** 1 mM CoA, or **(D)** 10 mM pyruvate. EPR parameters: spectral width, 2000 G; field center, 3400 G; modulation frequency, 100 kHz; modulation amplitude, 10 G; gain, 2×10^3; temperature, 10 K; microwave power, 2 mW; microwave frequency, 9.447 GHz.

of dimeric protein.[2] These results indicate that the *C. thermoaceticum* PFOR contains two Fe_4S_4 clusters/monomeric unit, as concluded earlier (Wahl & Orme-Johnson, 1987).

PFOR as isolated is EPR silent. Reduction of the enzyme was studied by EPR and UV−visible spectroscopy. When the enzyme was reacted with dithionite at pH 9.0, the EPR spectrum was complex with a double integral that corresponded to 3.9 spins/mol of dimeric enzyme, indicating that both clusters in the monomeric unit were fully reduced **(**Figure 2A). The spectral morphology is more complex than can be explained by simple rhombic signals, a characteristic of spin-coupled Fe_4S_4 clusters that are interacting through a dipolar coupling mechanism. This is a through space interaction that is observed when the two paramagnets are within approximately 10 Å. The multiplicity of observed signals is likely to arise from spin coupling between paramagnets. Similar features, including the broad peak at $g \approx 2.12$, appear in the spectra of fully reduced ferredoxins [see, for example, Baur *et al.* (1990)]. These spectra and the spin integration values are similar to those reported earlier for the dithionite-reacted enzyme (Wahl & Orme-Johnson, 1987). When the enzyme was reacted with pyruvate and CoA **(**Figure 2B), the EPR spectrum and the signal intensity were nearly identical to those of the dithionite-reacted enzyme with a double-integrated intensity that corresponded to 4.1 spins/mol of dimeric enzyme. Reaction of PFOR with CoA alone yielded an EPR spectrum with g values at 2.04, 1.94, and 1.89 **(**Figure 2C). The signal intensity corresponded to 2.0 spins/mol of dimeric enzyme, indicating

[2] Metals observed in amounts greater than 0.1 g atm/mol were Se (0.17), Mg (0.11), and Zn (0.16).

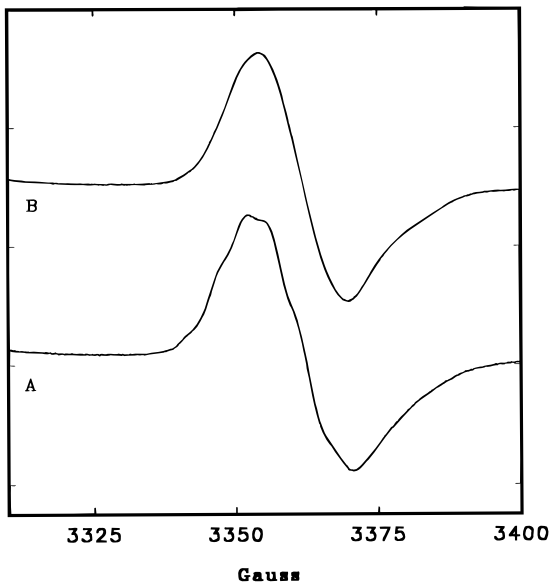

FIGURE 3: EPR signal of the HE−TPP radical intermediate. A solution containing 50 μM PFOR in buffer A in a final volume of 200 μL was incubated for 5 min at 25 °C with 10 mM **(A)** pyruvic acid, **(B)** CD_3-labeled pyruvic acid. EPR parameters: spectral width, 100 G; field center, 3360 G; modulation frequency, 100 kHz; modulation amplitude, 0.5 G; gain, 2×10^3; temperature, 10 K; microwave power, 2 mW; microwave frequency, 9.446 GHz.

that half of the Fe_4S_4 clusters had been reduced. This spectrum was similar to that observed previously for the partially reduced enzyme on photoreduction (Wahl & Orme-Johnson, 1987). Reaction of PFOR with pyruvate alone **(**Figure 2D) yielded an EPR spectrum consisting of two signals: an isotropic signal centered at $g = 2.008$ and a rhombic signal with g-values of 2.04, 1.94, and 1.89. We will refer to the EPR signal of the radical as the $g \approx 2.0$ signal. The double integrated intensity of the spectrum corresponded to 4 spins/dimeric enzyme with half of the spins residing in a Fe_4S_4 cluster and half in the radical species. Earlier it was reported that reaction of the *C. thermoaceticum* PFOR with pyruvate alone did not elicit any EPR signals (Wahl & Orme-Johnson, 1987). We cannot explain the discrepancy; however, we have obtained the same EPR spectrum numerous times with many samples of PFOR. The EPR signal of the cluster is complex, indicating that reduced cluster A and the HE−TPP radical are close enough to experience dipolar interactions (below). Similar conclusions were drawn based on EPR studies of the *H. salinarium* enzyme (Cammack *et al.*, 1980; Kerscher & Oesterhelt, 1981, 1982). We suggest that cluster A corresponds to the single cluster that is present in the *H. salinarium* enzyme.

For clarity, we introduce a working model in which we define the clusters that are reduced by pyruvate and CoA as clusters A and B, respectively. This is supported by the EPR experiments just described and stopped flow kinetic studies (below) that demonstrate that the optical absorption bands from the clusters undergo bleaching in two discrete phases.

As described below, the $g \approx 2.0$ EPR signal disappears quickly when the enzyme is reacted with both CoA and pyruvate; however, it is relatively stable when reacted with only pyruvate, allowing it to be unambiguously characterized as a substrate-derived radical. The enzyme was reacted with pyruvate and the EPR spectrum was scanned at low modulation amplitudes in the $g \approx 2.0$ region to detect hyperfine interaction with weakly interacting nuclei **(**Figure 3A). The

crossover point was measured to be at $g = 2.0080$ (± 0.0001). The EPR spectrum was similar to that of the *H. salinarium* enzyme, with a hyperfine splitting pattern that had been proposed to result from interactions between the unpaired electron and the three protons on carbon 3 of pyruvate (Kerscher & Oesterhelt, 1981, 1982). This signal was confirmed to be substrate-derived by reacting the enzyme with CD_3-pyruvate **(**Figure 3B). The predominant splittings observed in the pyruvate-reacted enzyme were altered when the C-3 protons (nuclear spin $I = 1/2$) were substituted with deuterons ($I = 1$). However, there are other features that appear to remain that may be due to interaction with other nuclear spins (such as the thiazole nitrogen). Further studies are required to assign the structure of this radical intermediate.

The UV−visible spectrum of the enzyme was similar to that described earlier (Wahl & Orme-Johnson, 1987). The extinction coefficients (ϵ) for the oxidized dimeric enzyme at 280 nm (220×10^3 M^{-1} cm^{-1}) and 390 nm (76.7×10^3 M^{-1} cm^{-1}) were only slightly different from those determined earlier by Wahl and Orme-Johnson (1987) and were found to be the same among six independent enzyme preparations. The difference extinction coefficient ($\Delta\epsilon$) at 420 nm (where the largest absorption change occurs) for the oxidized minus the reduced enzyme was 29.6×10^3 M^{-1} cm^{-1}/dimeric enzyme. If there are four clusters/dimer, this would correspond to a $\Delta\epsilon_{420}$ of 7.4×10^3 M^{-1} cm^{-1}/cluster. This is consistent with the presence of two Fd-like clusters/monomer since the ϵ_{390} and the $\Delta\epsilon_{420}$ for the 8-Fe Fd from *C. thermoaceticum* are 30 mM^{-1} cm^{-1} and 15 mM^{-1} cm^{-1}, respectively (Elliott & Ljungdahl, 1982).

Rapid Kinetic Studies. Rapid kinetic studies were performed to understand the mechanism of pyruvate decarboxylation by PFOR. FQ-EPR studies formed the basis of our mechanistic studies since the HE−TPP radical and the Fe_4S_4 clusters are EPR active. Potentially all the elementary steps in the mechanism (Figure 1) can be identified and their rates of formation and decay can be measured by FQ-EPR. However, since FQ-EPR is a discontinuous method and requires large amounts of enzyme, the precision by which rate constants can be measured is limited by the number of samples that can be analyzed. Generally, ~10 samples were used to define a kinetic trace. On the other hand, the stopped-flow method is continuous allowing 1000 data points to be collected in a single experiment. Thus, highly accurate rate constants can be measured for processes that result in optical spectroscopic changes, such as FeS cluster oxidation and reduction (apparently formation of the HE−TPP radical is not associated with measurable changes in the UV−visible region). Therefore, stopped-flow spectroscopic studies were used to augment the FQ-EPR studies. The value of k_{cat} for steady-state turnover is 33 s^{-1} at 25 °C, so any rate constant that is smaller than this value can be considered to be catalytically irrelevant.

Reaction with Pyruvate Only. When pyruvate and CoA were reacted with PFOR, the enzyme was completely reduced and the radical rapidly formed and decayed (below). Significant EPR signal intensity of the radical was present for less than 100 ms. To better characterize the radical and to understand the PFOR mechanism, FQ-EPR and stopped flow kinetic studies were performed by reacting PFOR with pyruvate in the absence of CoA (Figures 4−6). Two phases with widely different rate constants were detected by FQ-EPR**.** The first phase is shown in Figure 4. The second phase, shown in Figure 6, is too slow to be kinetically relevant. The EPR-monitored formation of the HE−TPP

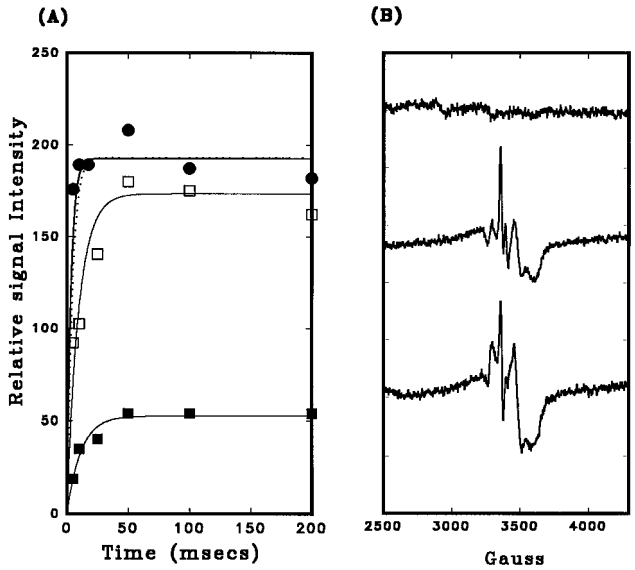

FIGURE 4: Reaction of PFOR with pyruvate studied by FQ-EPR. A solution containing 100 μM PFOR in buffer A was mixed with an equal volume of 10 mM pyruvic acid in the same buffer. **(A)** The intensities of the resonances at $g = 2.00$ (●), $g = 1.94$ (□), and $g = 2.04$ (■) were plotted as a function of time and fitted to single-exponential equations yielding rate constants of 190 ± 40 s^{-1}, 105 ± 35 s^{-1}, and 90 ± 18 s^{-1}, respectively. The EPR parameters were identical to those given in the legend to Figure 1 except that the microwave frequency was 9.448 GHz. (B) Representative EPR spectra at 0, 5, and 50 ms.

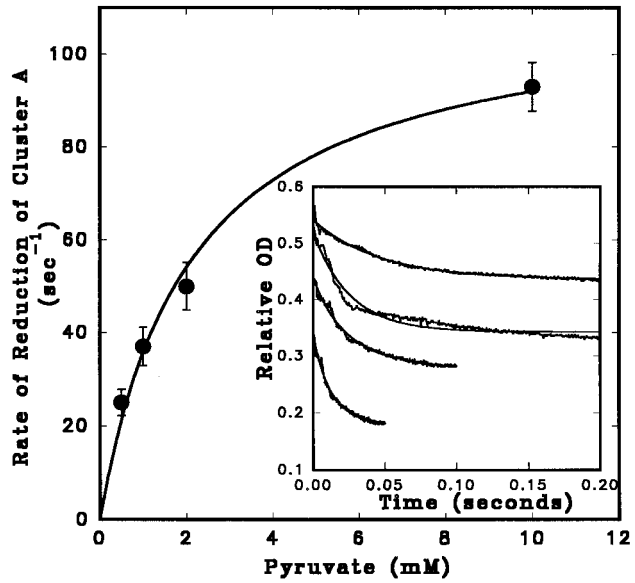

FIGURE 5: Pyruvate dependence of the rate constants for reduction of cluster A. A solution containing 10 μM PFOR in buffer A in one tonometer was rapidly mixed in a stopped-flow spectrometer at 25 °C with a solution containing pyruvate in buffer A in another tonometer. The reaction was monitored at 420 nm. The values for the rate constants were obtained by fitting the data to a single-exponential decay curve. The solid line was obtained by fitting the data to the Michaelis−Menten equation yielding values of K_m for pyruvic acid of 2.0 ± 0.3 mM and maximum k_{obs} of 98 ± 4 s^{-1}. **(**Inset) Individual stopped-flow traces obtained from reaction of PFOR with 0.5, 1, 2, and 10 mM pyruvate. The stopped flow traces were fit to the first half of the mechanism shown in Scheme 1. The stopped-flow traces were then simulated (solid lines) using the following derived rate constants: $k_{+1} = 860 \pm 40$ M^{-1} s^{-1}, $k_{-1} = 1590 \pm 80$ s^{-1}, $k_{+2} = 108 \pm 2$ s^{-1}, and $k_{-2} = 10.8 \pm 0.4$.

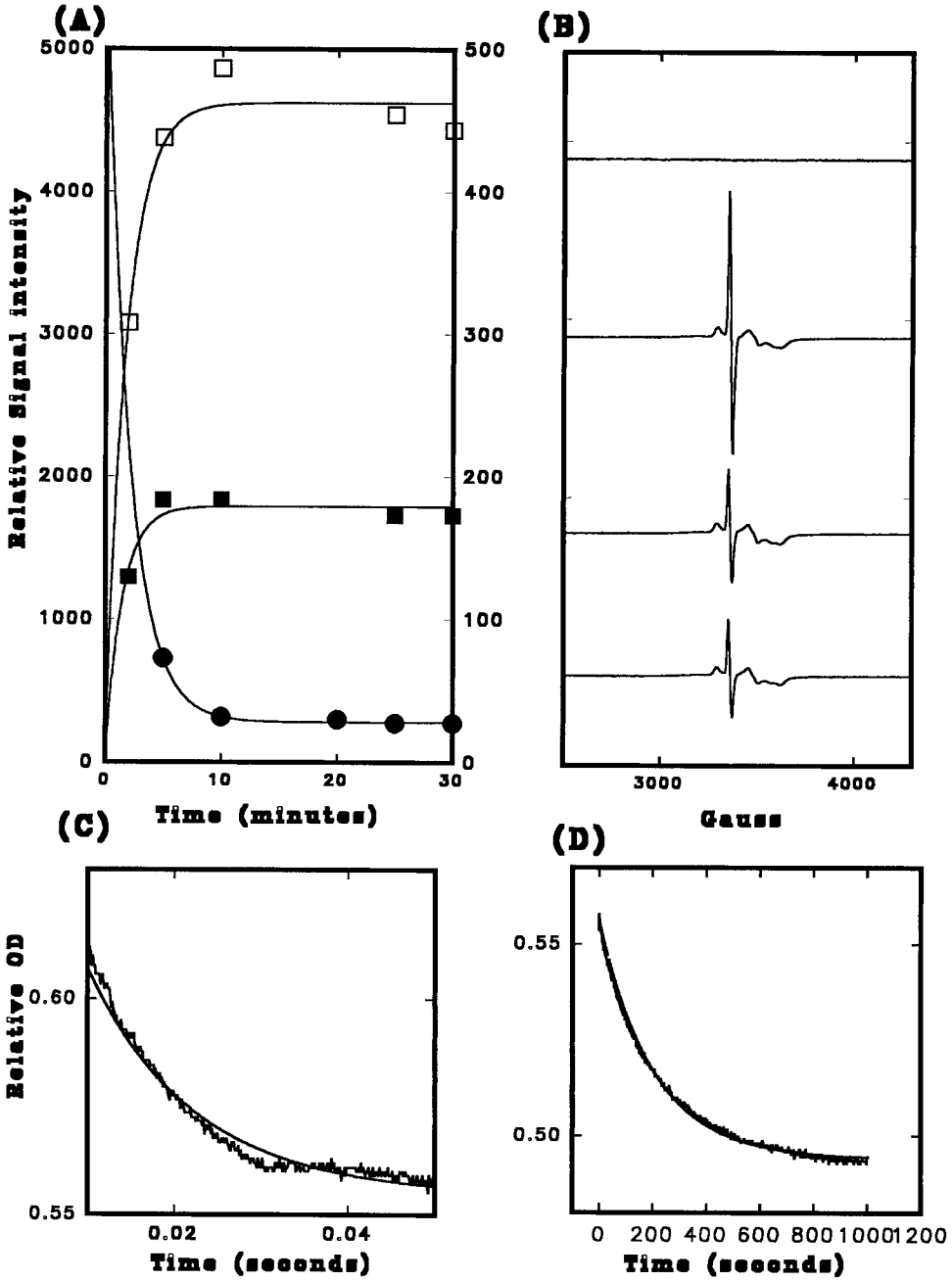

FIGURE 6: Slow decay of the HE−TPP radical coupled to reduction of cluster B. (A) A solution containing 50 μM PFOR in buffer A in a final reaction volume of 200 μL was reacted with pyruvate (10 mM, final), and the reaction was quenched at different times by freezing the EPR tube in liquid nitrogen. The intensity of the $g \approx 2.0$ signal (●) was plotted as a function of time and fitted to a single-exponential decay curve. The intensities of the resonances at $g = 2.04$ (■) and $g = 1.94$ (□) were plotted as a function of time and fitted to single-exponential equations. The solid lines were generated from the fits yielding rate constants of 0.008 ± 0.001 s^{-1} for the decay of the $g \sim 2.0$ signal and 0.009 ± 0.002 and 0.008 ± 0.001 s^{-1} for the increased intensity of the resonances at $g = 2.04$ and $g = 1.94$, respectively. The EPR parameters were identical to those given in the legend to Figure 1. (B) Representative EPR spectra at 0, 5, 10 and 25 min (upper to lower). (C) Rapid reduction of cluster A. A solution containing 5 μM PFOR in buffer A in one tonometer was rapidly reacted against 10 mM pyruvate in another tonometer at 25 °C, and the reduction of the cluster was followed at 420 nm. The calculated rate constant was 93 ± 1 s^{-1}. (D) Slow reduction of cluster B was monitored by stopped-flow spectroscopy as in Figure 5C except that a longer time base was used. The rate constant obtained from fitting the data to a single-exponential decay curve was 0.0075 ± 0.0005 s^{-1}. With 10 μM PFOR, the rate constants were nearly the same as with 5 μM−95 s^{-1} and 0.007 s^{-1}, for the fast and slow phases, respectively.

radical (Figure 4A, upper trace, solid line) and reduction of one of the two Fe_4S_4 clusters (Figure 4A, lower two traces, solid lines) both fit single-exponential equations. Formation of the radical ($k_{obs} = 190$ s^{-1}) appeared to be slightly faster than the rate of Fe_4S_4 cluster reduction ($k_{obs} = 105$ s^{-1}); however, more rigorous analysis (below) strongly indicates that radical formation and cluster reduction occur at the same rate. Double integration of the EPR spectrum when the signals reached maximum intensity yielded a value of approximately 4 spins/mol of dimeric enzyme,[3] consistent with one spin residing in the radical and one in the FeS cluster. Although the EPR signal clearly derives from a

[3] Given the relatively large standard deviations (20−30%), the rate constants for radical formation and cluster reduction are assumed to be equivalent. This simplifying assumption is supported by kinetic studies described later. It is impossible to accurately perform spin quantitation by FQ-EPR since the amount of isopentane (~30%) varies slightly for each packed sample.

Scheme 1

$$E + A \underset{k_{-1}}{\overset{k_1}{\rightleftharpoons}} EA, \quad EA \underset{k_{-2}}{\overset{k_2}{\rightleftharpoons}} F, \quad F + B \underset{k_{-3}}{\overset{k_3}{\rightleftharpoons}} FB, \quad FB \underset{k_{-4}}{\overset{k_4}{\rightleftharpoons}} G + Q$$

A = pyruvate, B = CoA, Q = acetyl-CoA

E = $PFOR_{ox}$ (Clusters A and B oxidized)

F = $PFOR_{red}$ (containing HE-TPP radical and Cluster A_{red} and B_{ox})

G = $PFOR_{red}$ (containing Clusters A and B reduced)

Table 1: Summary of Rate Constants Obtained from Fitting the Stopped Flow and FQ-EPR Data[a]

rate constants	
k_{+1}	860 ± 40 mM^{-1} s^{-1}
k_{-1}	1590 ± 80 s^{-1}
K_d (pyruvate)	1.8 mM
k_{+2}	108 ± 2 s^{-1}
k_{-2}	10.8 ± 0.4 s^{-1}
k_{+3}	1630 ± 50 mM^{-1} s^{-1}
k_{-3}	7.4 ± 0.3 s^{-1}
K_d (CoA)	4.5 μM
k_{+4}	33.3 ± 0.2 s^{-1}
k_{-4}	10.8 ± 0.1 mM^{-1} s^{-1}

[a] The rate constants refer to the model described in Scheme 1.

substrate-derived radical, the relaxation properties are profoundly affected by proximity to the cluster. Since organic radicals relax slowly, they are generally fully saturated in the low microwatt power range at low temperatures. In contrast, the half-power of saturation for the HE−TPP radical was found to be 2.6 mW at 10 K; this is very similar to the value measured for the cluster (3.4 mW). The fully developed spectrum was similar to that shown in Figure 2D, although the signal intensity was not as high. The data shown in Figure 4 were fit using the program FITSIM to a mechanism that included the first two steps of Scheme I with rate constants (k_1, k_{-1}, k_2, and k_{-2}) defined in Table 1. Simulation of the kinetics according to this mechanism is shown by the dotted line in Figure 4A.

Stopped-flow spectroscopic studies were performed to assess the dependence of the rate of cluster A reduction on pyruvate concentration **(**Figure 5). This analysis is important because k_1 is a bimolecular rate constant. As seen with the EPR-monitored reaction, two phases with widely different rate constants were observed; however, only the first was kinetically relevant for the overall steady-state mechanism. The first rapid phase of the stopped-flow data fit to a single-exponential equation throughout the range of pyruvate concentrations and the dependence of k_{obs} on pyruvate concentration could be fit to a simple Michaelis−Menton equation giving a maximum rate constant at saturating concentrations of pyruvate of 98 s^{-1} and a K_m for pyruvate of 2 mM. The K_m value was identical to that determined earlier (Wahl & Orme-Johnson, 1987) and confirmed in our laboratory by steady-state kinetics. The stopped flow traces were fit to a mechanism that included the first two steps of Scheme 1 using the program FITSIM . The kinetic simulation using the same rate constants used to fit the EPR data is shown in the inset to Figure 5. The K_d for pyruvate derived from this analysis was similar to the K_m value.

The results of Figure 4 and 5 support the hypothesis that PFOR reacts rapidly with pyruvate (8.6×10^5 M^{-1} s^{-1}) to form an intermediate (presumably the hydroxyethylidene−TPP species) that loses one electron to reduce cluster A and yield the HE−TPP radical. The elementary rate constants for the steps leading to formation of the radical when only pyruvate was present were not altered by including CoA in the reaction (below), indicating that the reaction is ordered with pyruvate binding first and CoA second. The magnitude of the absorption change and the integrated intensity of the EPR spectra strongly support the proposal that pyruvate reduces only one of the two clusters (cluster A) during the first phase of the reaction.

After the rapid reduction of cluster A accompanying the formation of the HE−TPP radical, the EPR signal of the radical slowly decayed ($k_{obs} = 0.008$ s^{-1}) as signal intensity in the Fe-S cluster region increased ($k_{obs} = 0.008-0.009$ s^{-1}) **(**Figure 6, panels A and B). Bleaching of the Fe-S cluster absorption spectrum was also monitored by stopped-flow kinetics **(**Figure 6, panels C and D). Two phases of equal amplitude were evident: the rapid reduction of cluster A ($k_{obs} = 93$ s^{-1}) was followed by slow reduction of cluster B ($k_{obs} = 0.008$ s^{-1}). The second phase was much too slow to be kinetically competent during steady-state turnover since the k_{cat} is ∼33 s^{-1}.

Reaction with CoA. When oxidized PFOR was incubated with CoA in the absence of pyruvate, an EPR signal was observed with g values of 2.04, 1.94, and 1.89. This spectrum is similar to that of cluster A; however, based on kinetic considerations described below, we will term this cluster B **(**Figure 1C). Double integration of the spectra yielded a spin concentration of 2 spins/mol of dimeric enzyme. Thus, CoA is capable of reducing one Fe_4S_4 cluster/monomer. We were unable to detect the formation of any other paramagnetic species. The time course of reduction of the enzyme by CoA was followed by stopped-flow kinetics **(**Figure 7). Each of the traces fit single-exponential equations over the range of CoA concentrations used. The magnitude of the absorption changes were consistent with the EPR results that one FeS cluster/monomer underwent reduction by CoA. The k_{obs} for reduction of cluster B was found to depend on the CoA concentration (Figure 7, inset); the K_m value was 4 μM and, at saturating concentrations, the observed rate constant was 35 s^{-1}, which is slightly faster than the steady-state k_{cat} (Menon & Ragsdale, 1996a). The K_m value is identical to that obtained previously by steady-state kinetics (Wahl & Orme-Johnson, 1987).

The stopped flow traces were fit using the program FITSIM to a two-step mechanism that included binding of CoA followed by reduction of cluster B (steps 3 and 4 of Scheme 1) with rate constants (k_3, k_{-3}, k_4, and k_{-4}) defined in Table 1. The kinetic simulations of the stopped-flow traces are shown in the inset to Figure 7. The K_d for CoA derived from the simulation (4.5 μM) is similar to the K_m value. As described below, the rate constants derived for this CoA-dependent step could be included in the overall four-step scheme. These data support a model in which pyruvate and CoA specifically reduce different clusters, clusters A and B, respectively.

Reaction with Pyruvate and CoA. When pyruvate and CoA were added to oxidized PFOR in the absence of an electron carrier, several intermediates were detected by FQ-EPR **(**Figure 8). First, EPR signals from the HE−TPP radical and a Fe_4S_4 cluster appeared, followed by decay of the radical signal and appearance of another Fe_4S_4 cluster signal. We concluded that the radical is identical to the one observed when PFOR was reacted with pyruvate alone

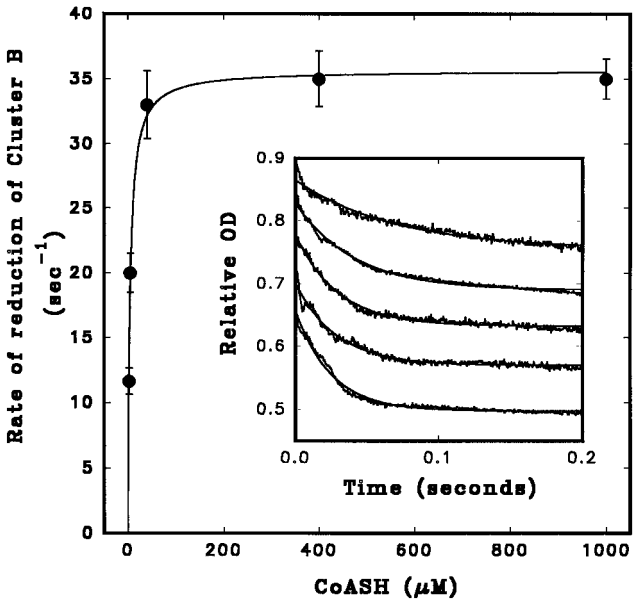

FIGURE 7: Reduction of cluster B by Coenzyme A. A solution containing 10 μM PFOR and buffer A in one tonometer was rapidly mixed at 25 °C with a solution containing 1 mM CoA in another tonometer and the reaction was monitored at 420 nm. The values for the rate constants, obtained from fitting the data to single-exponential equations, were plotted versus the CoA concentration and fit to a form of the Michaelis−Menten equation, giving a K_m for CoA of 4 ± 0.4 μM and a maximum k_{obs} of 35 ± 1 s^{-1} (Inset) Individual traces at 1, 2, 4, 400, and 1000 μM CoA. The stopped flow data were fit using KINSIM to a mechanism consisting of the third and fourth steps of Scheme 1. The solid lines shown in each of the traces were obtained by simulating the kinetic traces using the following derived rate constants: k_{+3} = 1630 mM^{-1} s^{-1}, k_{-3} = 7.4 s^{-1}, k_{+4} = 33.3 s^{-1}, and k_{-4} = 10.8 mM^{-1} s^{-1} (see Scheme 1).

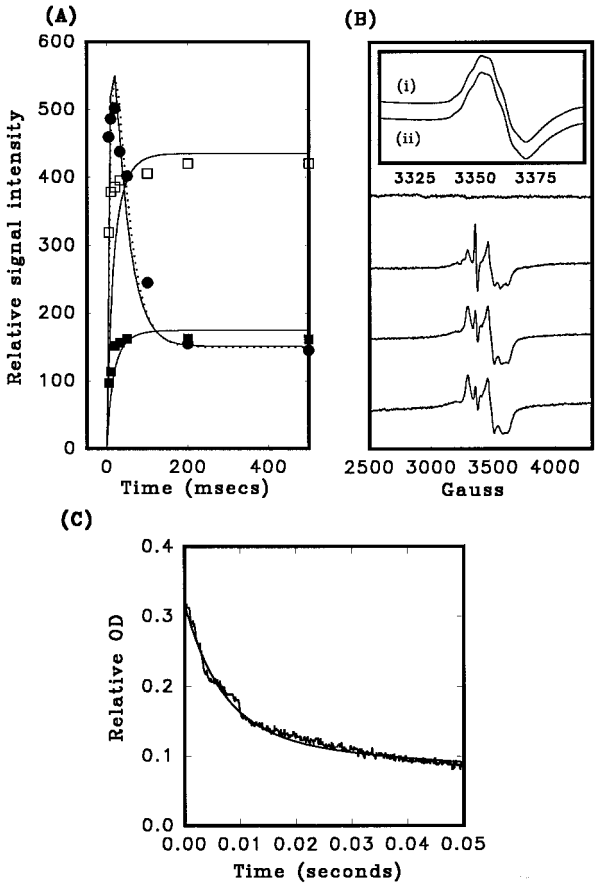

FIGURE 8: Reaction of PFOR with pyruvate and CoA. (A) A solution containing 100 μM PFOR in buffer A was rapidly mixed with a solution containing 10 mM pyruvic acid and 1 mM CoA in the same buffer, the reaction was quenched at different times by freeze quenching, and the samples were stored in liquid nitrogen and analyzed by EPR spectroscopy. The intensities of the resonances at g values of 2.00 (●), 1.94 (□), and 2.04 (■) were plotted as a function of time and fitted to double-exponential equations. The rate constants obtained for reduction of FeS clusters A and B (obtained from fitting the changes in intensity at g = 1.94 and g = 2.04) were 100 ± 10 and 35 ± 4 s^{-1}, respectively (solid lines). The rate constants for formation and decay of the radical (obtained from fitting the changes in the $g \approx 2.0$ signal intensity) were 98 ± 0.2 and 27 ± 1 s^{-1} (solid line). The data were fit to the mechanism described in Scheme 1 using FITSIM to yield the parameters described in Table 1. These values were then used in the KINSIM program to yield the simulation (dotted line). EPR parameters were the same as in Figure 1 except that the microwave frequency was 9.443 GHz. (B) Representative EPR spectra of samples quenched at 0 (before mixing), 5, 100, and 500 ms (upper to lower). (Inset) EPR spectra in the $g \approx 2.0$ region of (i) the FQ-EPR sample quenched after 150 ms of reaction with pyruvate and CoA and (ii) the sample reacted with pyruvate alone for 5 min. The EPR conditions were the same as those reported in Figure 3. (C) FeS cluster reduction followed by stopped-flow spectroscopy. A solution containing 10 mM PFOR in buffer A in one tonometer was rapidly mixed at 25 °C in a stopped-flow spectrometer with 10 mM pyruvate and 1mM CoA in another tonometer and the spectral changes due to reduction of the clusters at 420 nm was monitored. Fitting the data to a double-exponential equation with equal amplitudes in each phase gave values of 100 and 35 s^{-1}. The data were fit and simulated (solid line) with the rate constants shown in Table 1 as described in Figure 8A.

because the EPR spectra of the radicals formed under the two conditions were identical (Figure 8B, inset). This conclusion is reinforced by the kinetic study. The rate constants for radical formation and decay were first determined by fitting the data to a double-exponential equation, yielding rate constants of 98 and 27 s^{-1}, respectively.[4] Similar rate constants for the appearance of the EPR signals of clusters A and B were measured, 110 and 35 s^{-1}, respectively (Figure 8A, solid lines). The first rate constant is identical to that measured for formation of the radical and reduction of the cluster in the absence of CoA (*cf.* Figure 4); thus, CoA enhances the rates of radical decay and reduction of the second cluster, but has no effect on the rate of radical formation or reduction of cluster A. Equal EPR signal intensity was present in each of the two kinetic phases, indicating that one cluster /monomer underwent reduction in each phase. We analyzed the kinetics of radical formation and decay and reduction of clusters A and B (Figure 8A, dotted lines) by KINSIM and FITSIM according to the model described by Scheme 1 and including the eight rate constants defined in Table 1. For the FQ-EPR data, a relative amplitude of 917 obtained from the fit to the data was used. The observed maximum intensity was only 548; however, since the formation and decay of the radical are separated by rate constants that differ only by a third in magnitude, the radical signal can only partially accumulate.

The results of stopped-flow kinetics (Figure 8C) were consistent with the FQ-EPR results. The data were fit adequately by a double-exponential equation with rate

[4] That the radical does not completely decay is probably because reduction of cluster B by the HE−TPP radical is reversible. This interpretation is supported by recent studies that indicate that the midpoint potentials of the two clusters of PFOR are ∼−350 and −450 mV. Under steady-state conditions, complete decay of the radical would occur because reduction of the terminal electron acceptor (Fd, CODH, flavodoxin, etc.) would make the reaction irreversible.

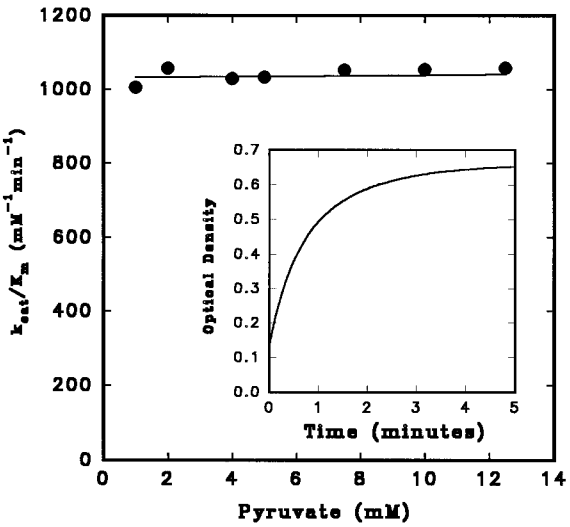

FIGURE 9: Determination of the k_{cat}/K_m for methyl viologen. The reaction mix contained 1 μM PFOR, 1 mM TPP, 1 mM CoASH, 50 μM methyl viologen, 50 mM Tris-HCl buffer (pH 7.5) and varying concentrations of pyruvic acid in a final reaction volume of 1 mL. The value of k_{cat}/K_m was 1020 $\pm$ 50 mM^{-1} min^{-1} or 1.7 ($\pm$0.1) $\times$ 10^4 M^{-1} s^{-1} at all concentrations of pyruvic acid tested. (Inset) A representative kinetic trace monitored at 604 nm following the complete reduction of methyl viologen with 4 mM pyruvic acid.

constants of 100 and 35 s^{-1}, including equal amplitudes in each phase. Analysis of the stopped-flow data was performed using the KINSIM and FITSIM programs **(**Figure 8C, dotted line) with the model and rate constants described above. The results of the stopped-flow experiments were entirely consistent with those obtained by FQ-EPR.

The model described in Scheme 1 is incomplete since it does not include the step for formation of the hydroxyethylidene−TPP intermediate. Since we did not have a way to monitor this step directly and did not want to add additional degrees of freedom to our simulations, we did not include it explicitly in the mechanism; however, since the data fit a mechanism that disregards this step, the rate of this reaction must be much faster than k_{+2}. Therefore, Scheme 1 includes four elementary steps: (i) binding of pyruvate, (ii) formation of the HE−TPP radical coupled to reduction of cluster A, (iii) binding of coenzyme A, and (iv) electron transfer from the radical resulting in reduction of cluster B. An important feature of our kinetic simulations is that a self-consistent set of rate constants could be used to fit all the FQ-EPR and stopped-flow data for the reactions of PFOR with pyruvate, with CoA, and with pyruvate and CoA. One simplification in the scheme is that k_{-2} was presented as a first-order rate constant since we did not attempt to follow the reaction in the reverse direction at varied CO_2 concentrations to obtain the proper second-order rate constant.

The model described in Scheme 1 and Figure 1 predicts that acetyl-CoA departs at the end of the first half-reaction and that there is a second half-reaction in which the reduced enzyme undergoes reoxidation by the terminal electron acceptor. If this is true, then the k_{cat}/K_m for the electron acceptor should be independent of the concentration of pyruvate. To test this hypothesis, we performed the reaction at low concentrations of methyl viologen and high varying concentrations of pyruvate **(**Figure 9). The reaction was followed to completion and the data were fit to eq 2. The viologen dye mediator was completely reduced demonstrating that, under these conditions, the reaction is irreversible.[5] The value of the k_{cat}/K_m for methyl viologen, 1.7 $\times$ 10^4 M^{-1} s^{-1}, was found to be the same over a 12-fold range in pyruvate concentration. A similar value for the k_{cat}/K_m for methyl viologen (3.0 $\times$ 10^4 M^{-1} s^{-1}) can be calculated from the values for k_{cat} (33 s^{-1}) and apparent K_m for methyl viologen (1.1 $\pm$ 0.1 mM), which were determined by performing initial velocity kinetics measurements at saturating concentrations of pyruvate. These results are consistent with the mechanism described by Scheme 1, in which PFOR is reduced at the end of the first half-reaction. In subsequent steps, the enzyme undergoes reoxidation by reaction with Fd, flavodoxin, CODH/ACS, or other electron acceptors (Menon & Ragsdale, 1996a), including protons when electron acceptors are not available (Menon & Ragsdale, 1996b).

DISCUSSION

Although many PFORs have been shown to contain more than two FeS clusters, apparently only two prosthetic groups are required for decarboxylation: TPP and one Fe_4S_4 cluster (Zhang *et al.*, 1996). Protein, iron, and sulfide determinations combined with kinetic and spectroscopic measurements strongly indicate that, in addition to TPP, the *C. thermoaceticum* enzyme contains two Fe_4S_4 clusters (designated clusters A and B)/120 kDa monomer in agreement with earlier studies on this enzyme (Wahl & Orme-Johnson, 1987). Adams and Kletzin proposed that there are two domains in PFORs that can house up to three Fe_4S_4 clusters: a γ domain consisting of two conserved $CX_2CX_2CX_3CP$ motifs that are characteristic for Fe_4S_4 clusters and a β domain with a different conserved four-cysteine motif near the proposed TPP binding site (Adams & Kletzin, 1996). The *H. salinarium* enzyme contains only the single cluster in the β domain and lacks the γ domain. It is likely that cluster A of the *C. thermoaceticum* PFOR is the one in the β domain since it exhibits spin-spin interactions with the radical, as was observed with the *H. salinarium* enzyme. Furthermore, cluster A is reduced simultaneously with formation of the radical. Although the sequence of the *C. thermoaceticum* PFOR is unknown, we suspect that a segment of the γ domain encoding the ligands for a Fe_4S_4 cluster has been deleted from the *C. thermoaceticum* PFOR gene. It is highly unlikely that a cluster was lost during purification because PFOR was purified under strictly anaerobic conditions and had a high specific activity. In addition, the extinction coefficients, k_{cat} values, EPR spectra and their spin intensities, and metal contents were the same in numerous preparations of PFOR. Furthermore, the rate constants for cluster reduction were faster than the steady-state k_{cat} and no further absorption changes were observed after the second cluster was fully reduced.

We used a combination of rapid kinetic and spectroscopic studies to elucidate the mechanism of the *C. thermoaceticum* PFOR. Figure 1 summarizes our conclusions. The first step that we could directly monitor spectroscopically was step 3, which involves one-electron transfer from hydroxyethylidene−TPP, leaving a radical and reducing cluster A. Our

[5] Irreversibility is expected based on the highly negative ΔG value for the reaction since the midpoint potentials for the acetyl-CoA/pyruvate and the MV_{ox}/MV_{red} couples are −540 mV (Thauer *et al.*, 1977) and −466 mV (Mayhew, 1978), respectively, and the pyruvate:MV_{ox} ratio is 200:1.

results provided unambiguous evidence that the radical is the substrate-derived radical that has been studied in other PFORs and assigned as a HE−TPP radical. This conclusion was based on the changes observed in the hyperfine splitting pattern when the protons at C-3 of pyruvate were replaced with deuterons. This experiment indicates that there is significant spin density among a number of atoms in the HE−TPP radical, *i.e.*, the radical is not purely oxygen centered as shown in Figure 1. That hyperfine broadened features remain in the spectrum obtained with fully deuterated pyruvate also indicates that other nuclei (perhaps the nitrogen of TPP) sense significant spin density. Studies are underway to try to assign a more satisfactory structure for the radical. Currently, there is controversy surrounding even the existence of this radical since it has been detected in some PFORs, but not in others. Why? It has been proposed that there are inherent differences among the PFORs in their cluster composition (Pieulle *et al.*, 1995) or in their reaction mechanisms (Blamey & Adams, 1993; Smith *et al.*, 1994). Since the HE−TPP radical was not detected in earlier studies of the *C. thermoaceticum* enzyme (Wahl & Orme-Johnson, 1987), it was classified as one of the nonradical enzymes. Our results strongly indicate that the reason that this radical is sometimes not detected is that it is a short-lived intermediate that would have decayed before the samples were frozen for EPR analysis. For example, when the *C. thermoaceticum* PFOR was reacted with pyruvate and CoA, the radical existed for only ∼100 ms. The best chance of observing this intermediate without using rapid kinetics is when the enzyme is reacted with pyruvate alone. However, even under these conditions, its lifetime was only ∼2 min.

Our results provide strong evidence that the HE−TPP radical is a catalytically relevant intermediate in the PFOR mechanism. This issue has not been addressed previously with any of the PFORs. When PFOR was incubated with pyruvate and CoA, the HE−TPP radical was shown to form faster ($k_{obs} = 100\ s^{-1}$) and to decay slightly faster ($k_{obs} = 35\ s^{-1}$) than the k_{cat} ($33\ s^{-1}$) for the formation of acetyl-CoA and CO_2 from pyruvate measured under steady-state conditions (Menon & Ragsdale, 1996a). Thus, the HE−TPP radical can be placed with confidence in the PFOR reaction mechanism, as shown in step 3 of Figure 1. On the basis of the considerations described above, we favor the recent suggestion that PFORs with different subunit compositions and different cluster compositions should have essentially the same catalytic mechanism (Zhang *et al.*, 1996), which will include the intermediacy of a HE−TPP radical. We argue that classification of PFORs based on the existence or lack of the HE−TPP radical is not justified and predict that the HE−TPP radical will be detected in all PFORs when rapid kinetics methods are used to follow the reaction.[6] PFOR thus joins the growing list of enzymes that generate radical intermediates derived from substrates, coenzymes, or amino acid residues (Stubbe, 1988).

Step 4 involves electron transfer from the HE−TPP radical to cluster B. We showed that the HE−TPP radical disappeared at the same rate that cluster B underwent reduction. Reduction of cluster B and radical decay occured at catalytically relevant rates only when CoA is present; in its absence, their rate constants were ∼4000-fold slower than k_{cat}. CoA could be viewed as controlling a gated electron transfer pathway from the radical to cluster B. How could CoA facilitate this reaction? One possibility is that CoA affects a pre-existing redox equilibrium between the HE−TPP radical and cluster B by specifically reacting with the form of PFOR in which cluster B is reduced. This could occur by a direct specific binding interaction with the reduced form of cluster B or by coupling a CoA-induced conformational change to alteration of the properties of cluster B. Another possibility is that thiolytic cleavage of the acetyl group is a very rapid and favorable reaction which pulls the slow redox interconversion between the HE−TPP radical and cluster B. Either of these possibilities constitute examples of the classical EC mechanism in which electron transfer is coupled to a chemical reaction. Therefore, by either of these scenarios, binding of CoA would be expected to increase the apparent redox potential of cluster B. This would increase the driving force for the electron transfer reaction and, consequently, increase the electron transfer rate. Evidence for the latter type of kinetic coupling is provided by studies of the *H. salinarium* PFOR, which contains a single cluster; Fd replaces the role of the second cluster (Kerscher & Oesterhelt, 1981). In this case, electron transfer from the radical to Fd was observed only in the presence of CoA. Since CoA binds to PFOR, not Fd, this indicates that rate acceleration is brought about by coupling thiolysis of the acetyl−TPP intermediate to the electron transfer reaction.

Another possibility is that CoA reduces cluster B directly, forming a CoA radical that could condense with the HE−TPP radical to form acetyl-CoA. There is evidence, based on spin trapping, for a CoA radical in the *Tritrichomonas foetus* PFOR reaction mechanism (Docampo *et al.*, 1987). In support of this possibility, CoA was found to specifically reduce cluster B, even when pyruvate is absent, at a rate that is approximately the same as that of steady state turnover (Figure 7). However, the one-electron reduction of cluster B should leave a CoA radical as the product; we have not observed any EPR signals that could be assigned to such a radical. Further experiments clearly are required to understand how CoA reacts with PFOR.

Step 5 completes the first half-reaction in the PFOR mechanism, yielding acetyl-CoA and the two-electron reduced enzyme. The acetyl-CoA is used both as a carbon and energy source by acetogenic bacteria. Completion of the catalytic cycle (step 6) requires the two-electron oxidation of PFOR by external electron acceptors, such as Fd, flavodoxin, CODH/ACS, or even protons when electron acceptors are limiting (Menon & Ragsdale, 1996b). The CO_2 generated in the early stages in the PFOR reaction can be reduced to CO by CODH/ACS, which is condensed with a bound methyl group and CoA to yield acetyl-CoA via the Wood/Ljungdahl pathway (Menon & Ragsdale, 1996a).

[6] However, sometimes catalytically competent intermediates are not observed because their formation rates are much slower than their decay rates.

REFERENCES

Adams, M. W. W., & Kletzin, A. (1996) *Adv. Protein Chem. 48*, 101−180.

Andreesen, J. R., Schaupp, A., Neurater, C., Brown, A., & Ljungdahl, L. G. (1973) *J. Bacteriol. 114*, 743−751.

Ballou, D. P. (1978) *Methods Enzymol. 54*, 85−93.

Barshop, B. A., Wrenn, R. F., & Frieden, C. (1983) *Anal. Biochem. 133*, 134−145.

Baur, J. R., Graves, M. C., Feinberg, B. A., & Ragsdale, S. W. (1990) *BioFactors 2*, 197−203.

Blamey, J. M., & Adams, M. W. W. (1993) *Biochim. Biophys. Acta 1161*, 19−27.
Bock, A.-K., & Schönheit, P. (1995) *J. Bacteriol. 177*, 2002−2007.
Bock, A.-K., Prieger-Kraft, A., & Schönheit, P. (1994) *Arch. Microbiol. 161*, 33−46.
Cammack, R., Kerscher, I., & Oesterhelt, D. (1980) *FEBS Lett. 118*, 271−273.
Cline, J. D. (1969) *Limnol. Oceanogr. 14*, 454−458.
Docampo, R., Moreno, S., & Mason, R. (1987) *J. Biol. Chem. 262*, 12417−12420.
Drake, H. L., Hu, S.-I., & Wood, H. G. (1981) *J. Biol. Chem. 256*, 11137−11144.
Elliott, J. I., & Brewer, J. M. (1978) *Arch. Biochem. Biophys. 190*, 351−357.
Elliott, J. I., & Ljungdahl, L. G. (1982) *J. Bacteriol. 151*, 328−333.
Fish, W. W. (1988) *Methods Enzymol. 158*, 357−364.
Heider, J., Mai, X., & Adams, M. W. W. (1996) *J. Bacteriol. 178*, 780−787.
Hrdy', I., & Müller, M. (1995) *J. Mol. Evol. 41*, 388−396.
Jones, J. B., Jr. (1977) *Commun. Soil Sci. Plant Anal. 8*, 349−365.
Kerscher, L., & Oesterhelt, D. (1981) *Eur. J. Biochem. 116*, 587−594.
Kerscher, L., & Oesterhelt, D. (1982) *Trends Biochem. Sci. 7*, 371−374.
Mai, X., & Adams, M. W. W. (1994) *J. Biol. Chem. 269*, 16726−16732.
Mayhew, S. G. (1978) *Eur. J. Biochem. 85*, 535−547.
Menon, S., & Ragsdale, S. W. (1996a) *Biochemistry 35*, 12119−12125.
Menon, S., & Ragsdale, S. W. (1996b) *Biochemistry 35*, 15814−15821.
Moulis, J. M., Davasse, V., Meyer, J., & Gaillard, J. (1996) *FEBS Lett. 380*, 287−290.
Pieulle, L., Guigliarelli, B., Asso, M., Dole, F., Bernadac, A., & Hatchikian, E. C. (1995) *Biochim. Biophys. Acta 1250*, 49−59.
Rajagopal, B. S., & LeGall, J. (1994) *Curr. Microbiol. 28*, 307−311.
Rupp, H., Rao, K. K., Hall, D. O., & Cammack, R. (1978) *Biochim. Biophys. Acta 537*, 255−269.
Segel, I. H. (1975) *Enzyme Kinetics*, John Wiley & Sons, San Francisco.
Seravalli, J. (1994) *Steady-state and time-dependent relaxation studies of the kinetics of action of lactate dehydrogenase from Bacillus stearothermophilus*, Ph.D Dissertation, University of Kansas, Lawrence, KS.
Smith, E. T., Blamey, J. M., & Adams, M. W. W. (1994) *Biochemistry 33*, 1008−1016.
Stubbe, J. (1988) *Biochemistry 27*, 3893−3900.
Thauer, R. K., Jungermann, K., & Decker, K. (1977) *Bacteriol. Rev. 41*, 100−180.
Wahl, R. C., & Orme-Johnson, W. H. (1987) *J. Biol. Chem. 262*, 10489−10496.
Zhang, Q., Iwasaki, T., Wakagi, T., & Oshima, T. (1996) *J. Biochem. (Tokyo) 120*, 587−599.
Zhao, S., Roberts, D. L., & Ragsdale, S. W. (1995) *Biochemistry 34*, 15075−15083.
Zimmerie, C. T., & Frieden, C. (1989) *Biochem. J. 258*, 381−387.

BI970403K